International Journal of Fluid Machinery and Systems
Vol. 7, No. 1, January-March 2014

DOI: http://dx.doi.org/10.5293/IJFMS.2014.7.1.016
ISSN (Online): 1882-9554

Original Paper

Predicting Double-Blade Vertical Axis Wind Turbine Performance by a Quadruple-Multiple Streamtube Model

Yutaka Hara[1], Takafumi Kawamura[2], Hiromichi Akimoto[3], Kenji Tanaka[4], Takuju Nakamura[5], and Kentaro Mizumukai[5]

[1]Department of Mechanical and Aerospace Engineering, Tottori University
4-101 Minami, Koyama-cho, Tottori 680-8552, Japan, hara@damp.tottori-u.ac.jp
[2]Computational Fluid Dynamics Consulting Inc.
2-1-1-1111 Namiki, Tokorozawa, Saitama 359-0042, Japan, kawamura@cfd-consulting.co.jp
[3]Division of Ocean Systems Engineering, KAIST
291 Daehak-ro, Yuseong-gu, Daejeon 305-701, Republic of Korea, akimoto@kaist.ac.kr
[4]Department of Systems Innovations, The University of Tokyo
7-3-1 Hongo, Bunkyo-ku, Tokyo 113-8656, Japan, tanaka@triton.naoe.t.u-tokyo.ac.jp
[5]New Business Development, MODEC Inc.
Nihonbashi Maruzen Tokyu Building, 3-10 Nihonbashi 2-chome, Chuo-ku, Tokyo 103-0027, Japan,
Takuju.nakamura@modec.com, kentaro.mizumukai@modec.com

Abstract

Double-blade vertical axis wind turbines (DB-VAWTs) can improve the self-starting performance of lift-driven VAWTs. We here propose the quadruple-multiple streamtube model (QMS), based on the blade element momentum (BEM) theory, for simulating DB-VAWT performance. Model validity is investigated by comparison to computational fluid dynamics (CFD) prediction for two kinds of two-dimensional DB-VAWT rotors for two rotor scales with three inner-outer radius ratios: 0.25, 0.5, and 0.75. The BEM-QMS model does not consider the effects of an inner rotor on the flow speed in the upwind half of the rotor, so we introduce a correction factor for this flow speed. The maximum power coefficient predicted by the modified BEM-QMS model for a DB-VAWT is thus closer to the CFD prediction.

Keywords: Wind turbine, Double-blade rotor, VAWT, BEM, CFD, QMS.

1. Introduction

Vertical axis wind turbines (VAWTs) offer lower costs due to the simplified mechanics, because the wind direction is unimportant to performance. However, small-scale lift-driven VAWTs typically have poor self-starting performance [1]. Therefore, a variety of steps have been tried to improve self-starting performance: increasing blade chord length, adding more blades, using drag-driven wind turbines as a starter, and designing blade airfoils for high aerodynamic performance (for example, [2]). Double-blade vertical axis wind turbines (DB-VAWTs), such as the one shown in Fig. 1 (a), are an example for improving self-starting performance. DB-VAWTs can produce larger starting torque than conventional single-rotor VAWTs with the same blade chord length. Figure 1(b) shows a new type of VAWT with multiple looped blades forming a double-blade rotor structure, as in a DB-VAWT. This VAWT was named the butterfly wind turbine (BWT) [3] because as it rotates around the vertical axis it has the shape of a butterfly. The BWT may offer reduced costs, good self-starting performance, high energy efficiency, and good vibration handling because of the direct installation of the armless looped blades on the central axis.

Although propeller-type horizontal axis wind turbines (HAWTs) are the primary turbines for large-scale wind power generation, large-scale VAWTs have been recently proposed and developed for offshore wind power because of their low operational and maintenance costs [4]–[10]. A large-scale VAWT requires struts or arms that connect the blades and central rotating axis, and the cross-section of the struts should also be airfoils to reduce drag. These airfoil struts produce lift force if they incline against the horizontal plane, and so the structure can be regarded as a partial double-blade rotor.

Since the flow field of a double-blade rotor is very complex, it is difficult to predict performance by using conventional blade

Received December 2 2013; revised January 17 2014; accepted for publication January 21 2014: Review conducted by Dr. Hideaki Tamaki. (Paper number O13031C)
Corresponding author: Yutaka Hara, Associate Professor, hara@damp.tottori-u.ac.jp

element momentum (BEM) theory. In the present paper, we propose a new flow field model, which we call the quadruple-multiple streamtube (QMS) model, for predicting the performance of double-blade rotors. The QMS model extends the double multiple streamtube model (DMS model) [11], which is based on the BEM theory. The validity of QMS modeling is investigated by comparison with computational fluid dynamics (CFD) results. Additionally, characteristics of double-blade VAWTs are investigated by simulating two sizes of outer rotor and varying the ratio of the inner rotor radius to the outer rotor radius in each case.

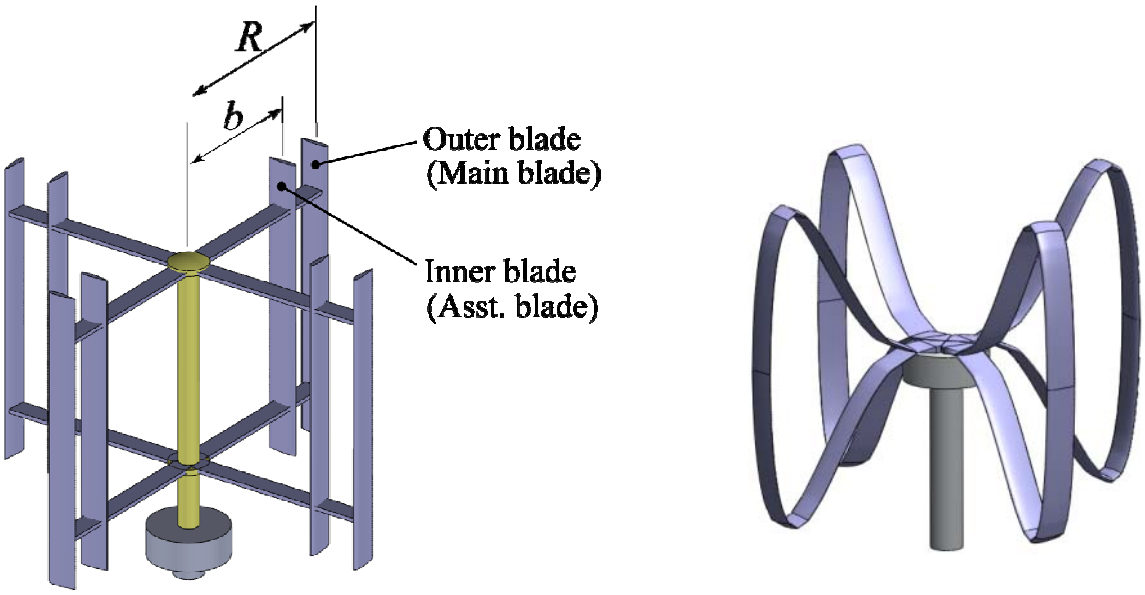

(a)DB-VAWT (b)BWT

Fig. 1 Double-blade vertical axis wind turbine (left) and butterfly wind turbine (right)

2. Predicting VAWT Performance

2.1 Quadruple-Multiple Streamtube Model

The DMS flow model [11] used in conventional BEM theory and the QMS flow model proposed in this paper are shown in Fig. 2. In the DMS model, with a_1 and a_2 as the induced-velocity factors in the upwind and downwind zones respectively, flow velocity is expressed as follows:

$$V_1 = V_0(1 - a_1) \tag{1}$$

$$V_{e12} = V_0(1 - 2a_1) \tag{2}$$

$$V_2 = V_{e12}(1 - a_2) \tag{3}$$

$$V_W = V_{e12}(1 - 2a_2) \tag{4}$$

Here, V_0 is the upstream uniform velocity and V_W is the rotor-wake velocity. V_{e12} is an equilibrium-induced velocity used as an input for the downwind zone.

In the double-blade rotor cases to which the QMS model is applied, fluid in a streamtube intersects rotor planes up to four times. When this is the case, by introducing a_1, a_2, a_3, and a_4 as the induced-velocity factors in each cross-section, flow velocity can be modeled as follows:

$$V_1 = V_0(1 - a_1) \tag{5}$$

$$V_2 = V_{e12}(1 - a_2) \tag{6}$$

$$V_3 = V_{e23}(1 - a_3) \tag{7}$$

$$V_4 = V_{e34}(1 - a_4) \tag{8}$$

$$V_W = V_{e34}(1 - 2a_4) \tag{9}$$

Here V_{e12}, V_{e23}, and V_{e34} are equilibrium-induced velocities; they are modeled as follows:

$$V_{e12} = V_0(1 - 2a_1) \tag{10}$$

$$V_{e23} = V_{e12}(1 - 2a_2) \tag{11}$$

$$V_{e34} = V_{e23}(1 - 2a_3) \tag{12}$$

On the basis of the BEM theory, each induced-velocity factor, which must satisfy both the momentum theory and the blade element theory at each cross section, is found by iterating to convergence. In the QMS model, the induced-velocity factors (i.e., velocities in a streamtube) are calculated in the order a_1, a_2, a_3, a_4, from the upstream side. Correspondence between the outer rotor (radius: R; azimuth: ψ_R) and the inner rotor (radius: b; azimuth: ψ_b) is given by

$$R\cos\psi_R = b\cos\psi_b \tag{13}$$

Some streamtubes in the double-blade rotor do not intersect the inner rotor. In such streamtubes, the DMS model is used instead to obtain the flow velocity.

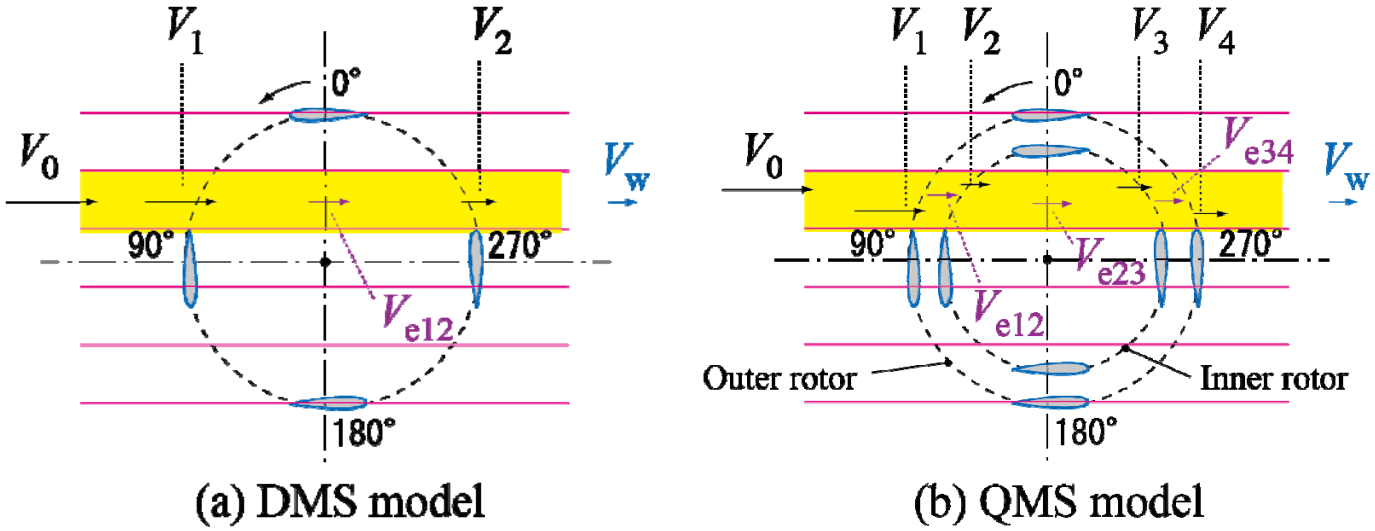

Fig. 2 (a) DMS model used for a conventional (single) rotor and (b) QMS model proposed for double-blade rotors

2.2 Simulated Rotors

Two rotors are selected for simulation in this study; these have different outer rotor diameters, as shown in Fig. 3. Both rotors are two-dimensional DB-VAWTs with three pairs of double blades; each pair consists of an outer blade and an inner blade. For the large-scale rotor (case A), the chord lengths of the outer and inner blades (c_1 and c_2) are 1 m and the radius of the outer rotor R is 10 m. The radius of the inner rotor b is 2.5 m, 5.0 m, or 7.5 m. The diameter D_a of the rotational axis is 1.5 m; this is considered in the performance calculations. For the small-scale rotor (case B), the chord lengths of the outer and inner blades (c_1 and c_2) are 0.2 m and the radius of the outer rotor R is 1 m. The radius of the inner rotor b is 0.25 m, 0.5 m, or 0.75 m. The diameter D_a of the rotational axis is assumed to be 0.15 m.

In this study, the blade sections are assumed to be symmetrical NACA 0018 airfoil for BEM calculations. However, to account for flow curvature effects [12], blade sections obtained by conformal mapping [13] of NACA 0018 airfoil to the curvilinear flow along the blade path are assumed in CFD analysis. That is, the present study assumes that the results of BEM calculation using symmetrical airfoil data correspond to the performance of a wind turbine rotor with cambered blades as obtained by transformation of the symmetrical airfoil to an equivalent curvilinear flow field. BEM and CFD calculations are two dimensional.

Although the supporting struts are not considered in the present calculations, the installation position of a blade on a virtual arm is assumed to be 25% of the chord length from the leading edge. The pitch angle of each blade at the blade installation position is tabulated in Table 1, together with camber for each blade and rotor condition. In the BEM calculations, for example, the pitch angle of the outer blade in case A was set at 1.43°; the corresponding value in case B was set at 2.87°. The upstream uniform flow velocity V_0 was assumed to be 10 m/s in this study.

2.3 Calculation by BEM-QMS

Performance of the double-blade rotors was simulated by the BEM theory with the QMS model (BEM-QMS), which was described in section 2.1. As a standard for comparison, the performance of a single rotor equivalent to the outer rotor was calculated in each case by the BEM theory using the conventional DMS model. The aerodynamic data of NACA 0018 presented

by Sheldahl and Klimas [14] were used as the input into an in-house program for VAWT performance prediction. However, aerodynamic data were replaced with the data presented by Kumar et al. [15] for cases in which there was both a low Reynolds number ($1.0\times10^4 \le Re \le 1.6\times10^5$) and a small angle of attack ($|\alpha| \le 25^\circ$). The modified Gormont model with $A_M = 6$ (Berg's modification [16]) was used in the dynamic stall model together with Paraschivoiu's modification [11], which replaces the dynamic stall model in the high turbulence range (105° to 225° in Fig. 2). However, to avoid discontinuity, our BEM-QMS program smoothly switches the dynamic stall model on and off at the boundary of the high turbulence range. For both the outer and inner rotors, the number of streamtubes is 36, in the direction normal to the mainstream. In the present BEM predictions, the effects of the rotor axis were considered by assuming the wake of a stationary cylinder.

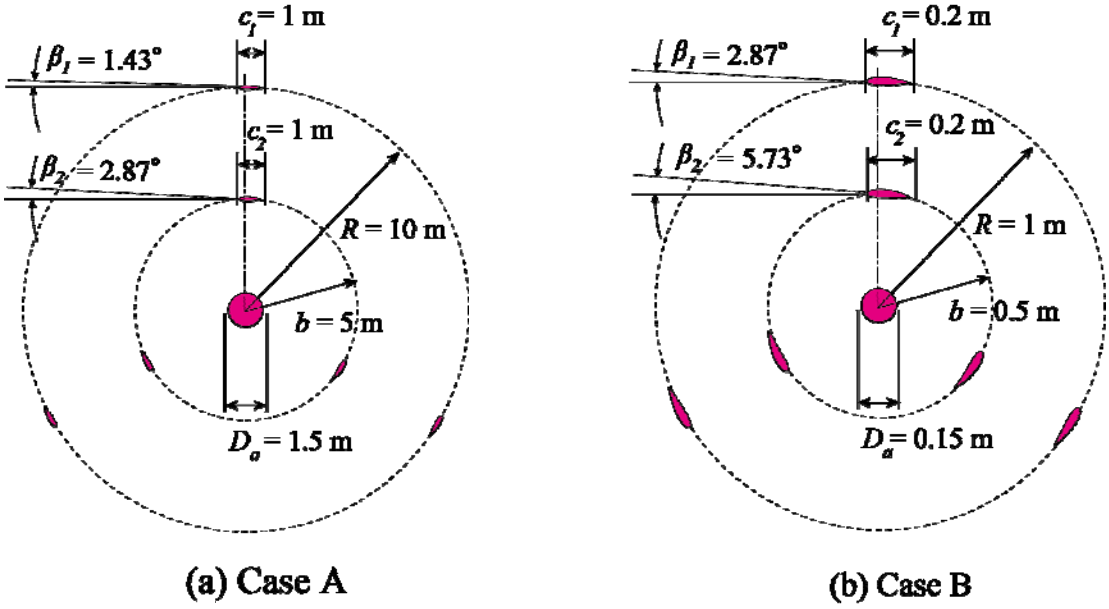

Fig. 3 Simulated objects. (a) case A: R = 10 m, $c_1 = c_2$ = 1 m; (b) case B: R = 1 m, $c_1 = c_2$ = 0.2 m

Table 1 Camber and pitch angle of each blade in each case

Case	Outer/Inner	*b*/*R*	Camber (%)	Pitch Angle: β (deg)
A	Outer	-	1.28	1.43
	Inner	0.75	1.71	1.91
	Inner	0.5	2.57	2.87
	Inner	0.25	5.15	5.73
B	Outer	-	2.57	2.87
	Inner	0.75	3.42	3.82
	Inner	0.5	5.15	5.73
	Inner	0.25	10.40	11.46

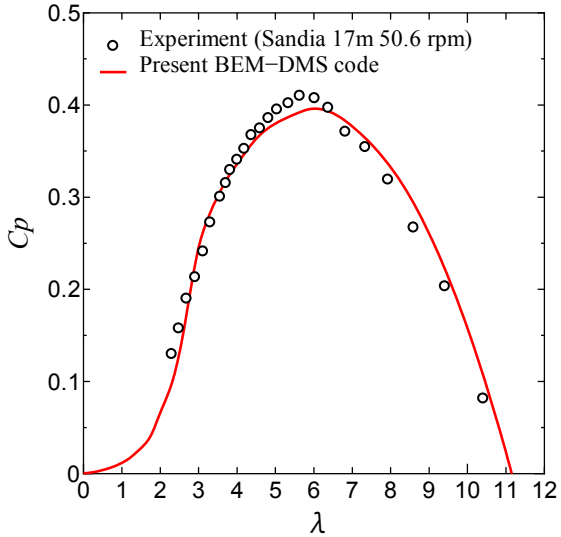

Fig. 4 Power characteristics of a 17 m Darrieus rotor. Both simulated data by BEM-DMS and experimental data are shown.

Results of predicting the power characteristics of a 17 m Darrieus rotor (Sandia Corporation) by using our BEM program are shown in Fig. 4, which also shows a plot of experimental data at constant rotational speed of 50.6 rpm [17]. The blade airfoil of the 17 m rotor is NACA 0015 and the aerodynamic data given by Sheldahl and Klimas [14] were used for the BEM prediction in Fig. 4. The BEM prediction for the 17 m rotor was a three-dimensional calculation, with vertical division into 21 levels. For each level, the DMS model was used to obtain the velocity field and the aerodynamic forces of the blades; these forces were numerically integrated to obtain the whole rotor performance. As shown in Fig. 4, the prediction by our BEM program agrees well with the experimental results over a wide range of tip speed ratios.

2.4 Calculation by CFD

To validate the BEM-QMS model, two-dimensional CFD analysis was conducted. The simulation objects are two sizes of double-blade rotors, described as cases A and B above (Fig. 3), a single rotor with outer radius 10 m, and a single rotor with outer radius 1 m; these sizes correspond to the outer rotor sizes of cases A and B, respectively. Examples of the generated meshes are shown in Fig. 5. In case A, the calculation domain consisted of a region of motion (a circle with radius of 12 m) and a static region (a 960 m × 1280 m rectangle). The calculation domain in case B was a 1:10 scale version of the calculation domain in case A. The size of the calculation domain and the resolution of the mesh were chosen to have minimal impact on the results. The CFD solver used was ANSYS Fluent v13; the QUICK scheme was used for the momentum equation, and the secondary accuracy scheme was chosen for the pressure equation. Time integration was performed by a second-order implicit method, and the SST-k-ω turbulence model was used; the size of the time step was set to the time in which a rotor revolves one degree. The number of cells was about 260,000 in the region of motion and about 40,000 in the static region. Each calculation was carried out up to five complete revolutions of the rotor, and the power and torque coefficients were obtained by averaging the power and torque during the last revolution.

Figure 6 illustrates the results of case A with inner-outer radius ratio b/R = 0.5 and tip speed ratio of 4; panel (a) shows the distribution of the streamwise velocity component, and panel (b) shows the distribution of vorticity component. From these, it can be seen that the streamwise velocity greatly decreases within the radius of the inner rotor and its wake, and the outer rotor blade moving in the downwind side traverses the vortices ejected by the inner rotor blades.

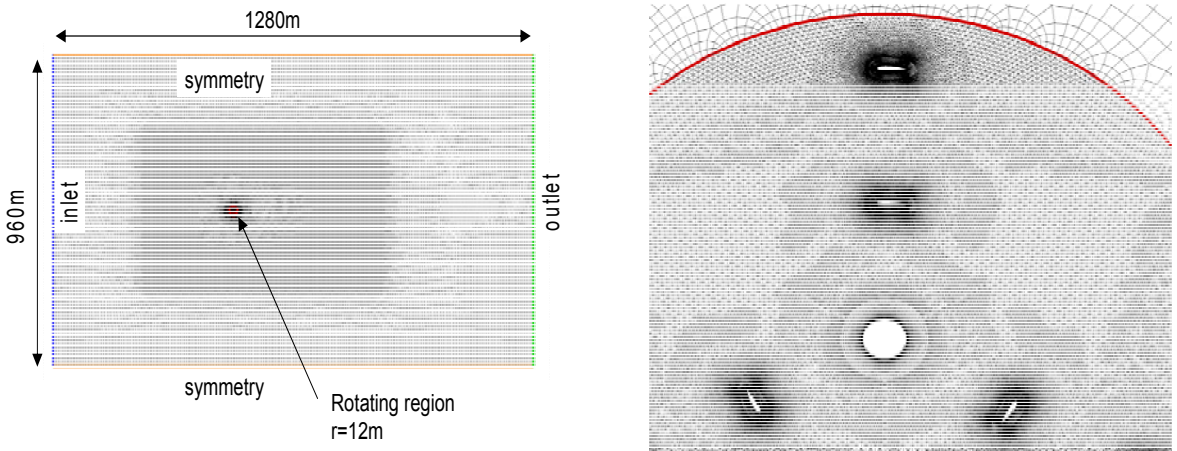

(a) Overall calculation region (b) Rotating region (Case A, b/R = 0.5)

Fig. 5 Examples of generated mesh for 2D CFD analyses

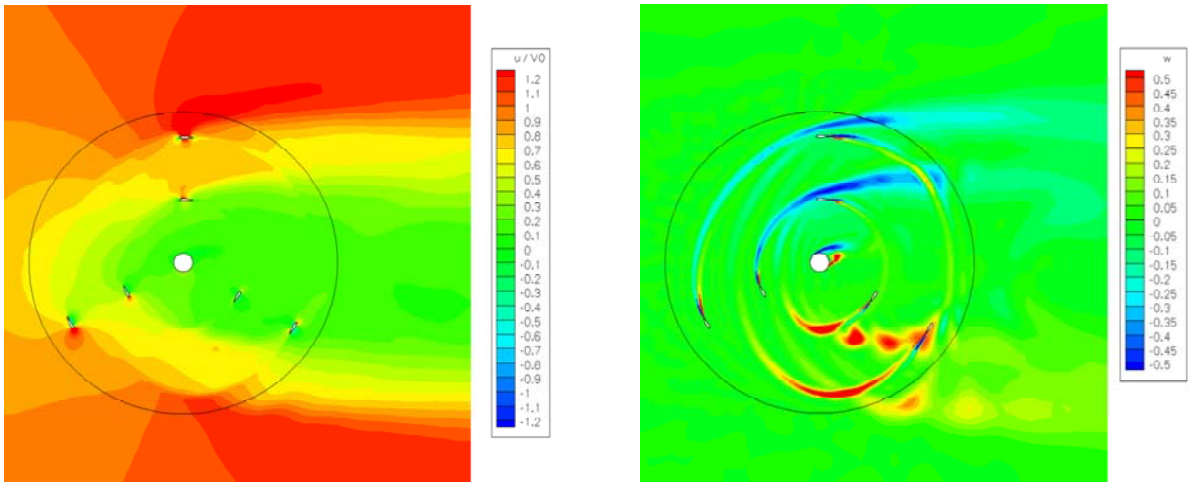

(a) Distribution of streamwise velocity component (b) Distribution of vorticity component

Fig. 6 Two-dimensional CFD analysis for case A with b/R=0.5 and tip speed ratio 4

3. Results

3.1 Comparison between BEM-QMS and CFD

Figure7 shows a comparison between BEM-QMS and CFD results obtained for the total power coefficients of double-blade rotors; panels (a) and (b) show cases A and B, respectively. The power characteristics of single rotors in both cases are also shown in Fig. 7 for comparison. The BEM and CFD predictions agree well on the maximum power coefficient of the single rotor in case A. However, the predicted tip speed ratio at which the maximum power coefficient will be obtained in BEM predictions is higher than that in CFD predictions. Differences between BEM and CFD predictions for a single rotor tend to grow as rotor size is decreased; this is shown in Fig. 7(b), which shows results for case B. The causes of this discrepancy on small-scale rotors are not yet clear. Possible causes include the dynamic stall model (or the selection of the A_M parameter) and the aerodynamic data at low Reynolds numbers. For example, the blade Reynolds number at tip speed ratio $\lambda = 3$ in case A is between 1.3×10^6 and 2.6×10^6 ; in case B the same tip speed ratio gives a Reynolds number between 2.6×10^5 and 5.3×10^5.

The difference between BEM-QMS and CFD predictions for double-blade rotors are large in both case A and case B. The maximum power coefficient predicted by CFD decreases greatly with increasing inner-outer radius ratio. However, the BEM-QMS prediction shows a small decrease in the maximum power coefficient. Nevertheless, the predictions by BEM-QMS and CFD agree qualitatively: the power coefficient increases at lower tip speed ratios and decreases at higher tip speed ratios with increasing inner-outer radius ratio.

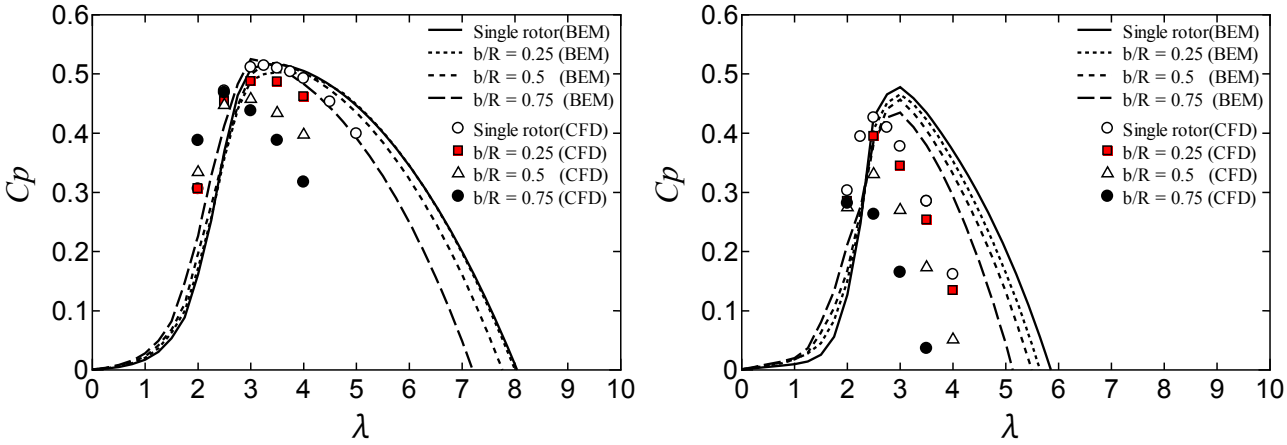

(a) Case A (large rotor) (b) Case B (small rotor)

Fig. 7 Total power coefficients vs. tip speed ratio in (a) case A and (b) case B

Figures 8 and 9 show the contributions from the outer and inner rotors to the torque coefficient. Despite some differences in the tip speed ratio at peak torque, the maximum torque coefficients of the outer rotor approximately agree between the BEM-QMS and CFD predictions in case A for each inner-outer radius ratio (Fig. 8(a)). In case B (Fig. 8(b)), the maximum torque coefficient of the outer rotor for $b/R = 0.25$ almost agrees between the BEM-QMS and CFD predictions, but the difference between the predictions grows as the value of b/R increases. As seen for power coefficients, the tip speed ratios corresponding to the maximum torque coefficients are higher in BEM-QMS predictions than in CFD predictions.

Predicted torque coefficients of the inner rotor in case A agree well for tip speed ratios between 3 and 4 when the inner-outer radius ratio is 0.75 or 0.5 (see Fig. 9(a)). In contrast to the outer rotor torque coefficients, the tip speed ratio predicted by BEM-QMS as giving the maximum torque coefficient of the inner rotor increases with decreasing the value of b/R in case A; yet, the tip speed ratio for torque peak, as predicted by CFD, does not depend on b/R in Fig. 9(a). In Fig. 9(b), showing case B, the inner-rotor torque coefficients from BEM-QMS predictions have two peaks; this is likely due to dynamic stall effects. Although an exact judgment is impossible due to the small number of CFD predictions, the CFD results seem to decrease monotonically between $\lambda = 2$ and $\lambda = 3$ (Fig. 9(b)). Except for these details, the BEM-QMS and CFD predictions for the inner-rotor torque coefficients coincide quantitatively in case A and case B.

We now compare the BEM-QMS and CFD predictions on variation of torque exerted on a blade as a function of that blade's azimuth. The analysis techniques are two dimensional, which we address by defining the non-dimensional torque CQ (blade torque coefficient) by using the torque Q exerted on a blade with unit height; this is calculated as follows:

$$CQ = \frac{Q}{0.5\,\rho V_0^{\,2}\,DR} \tag{14}$$

where ρ is air density and D is the outer rotor diameter ($D = 2R$).

Figure 10 shows the predicted torque variations for one blade in the single rotor case. The difference between BEM and CFD predictions is large when the azimuth is between 0° and 120°; this is true for both large and small rotors. In this azimuth range, blades move upstream in the upwind half-cycle and flow is not turbulent. The BEM calculations do not consider secondary flow. However, the CFD predictions show the effects of secondary flow, which are especially illustrated by the shift in the position of

torque-dip (azimuth of around 270° in Fig. 10) caused by the wake of the rotational axis. The difference between BEM and CFD predictions may arise from these secondary flow effects. Because the angle of attack is large when azimuth is between 30° and 120°, the choice of dynamic stall model might also be reflected in prediction differences. Although there are some differences between predictions for other ranges of azimuth, as shown in Fig. 10, overall, predictions of torque variations of single rotors agree between the BEM and CFD methods when tip speed ratio is 3.

Blade torque coefficients *CQ* of the double-blade rotor in case A with $b/R = 0.75$ at tip speed ratio 3 are shown in Fig. 11. In Fig. 11(a), the *CQ*s of the outer and inner rotors predicted by BEM-QMS are compared to the *CQ* of the single rotor. In Fig. 11(b), the *CQ*s predicted by CFD are compared similarly. The *CQ* of the outer rotor predicted by BEM-QMS is the same as the *CQ* of the single rotor for azimuth from 0° to 180°. This shows that the BEM-QMS model did not reflect the drop in upstream velocity

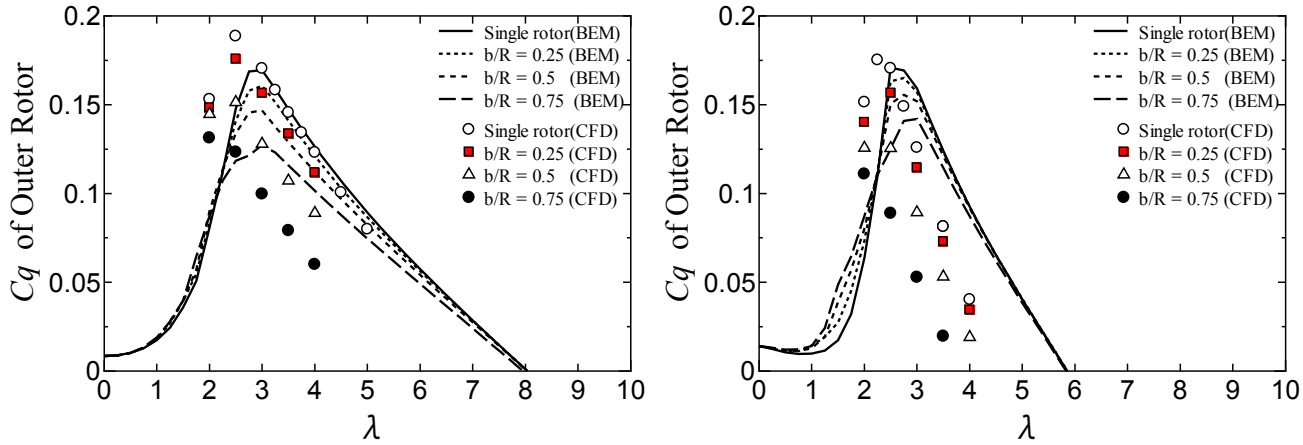

(a) Case A (large rotor) (b) Case B (small rotor)

Fig. 8 Torque coefficients of outer rotors in (a) case A and (b) case B

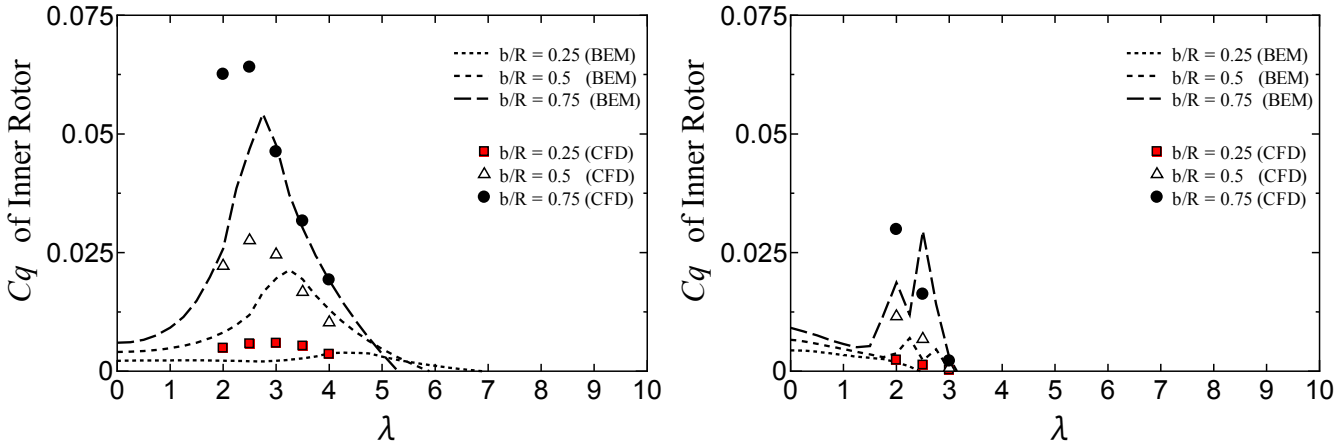

(a) Case A (large rotor) (b) Case B (small rotor)

Fig. 9 Torque coefficients of inner rotors in (a) case A and (b) case B

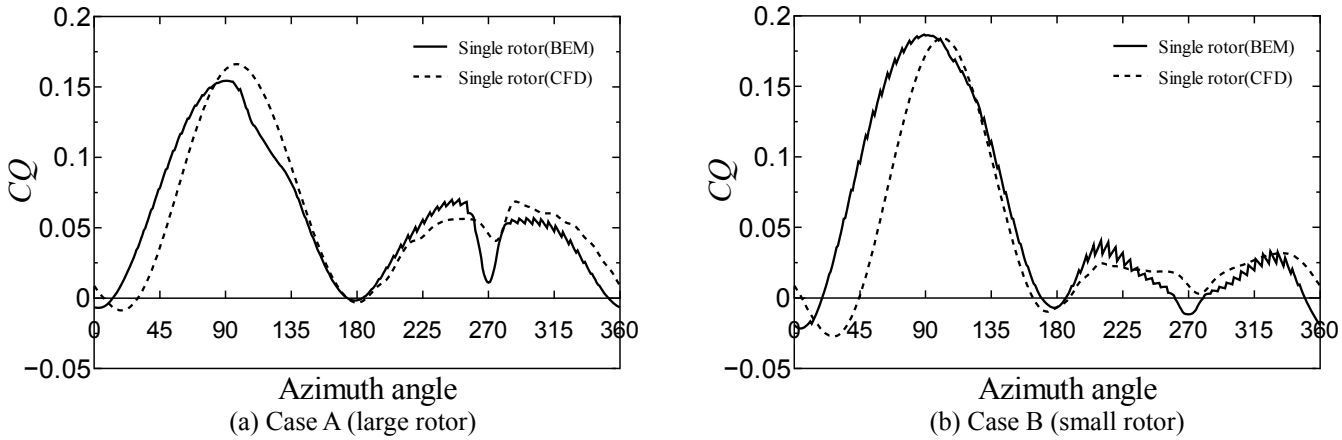

(a) Case A (large rotor) (b) Case B (small rotor)

Fig. 10 Blade torque coefficient *CQ* of a single rotor for λ=3 and rotor radius (a) 10 m and (b) 1 m.

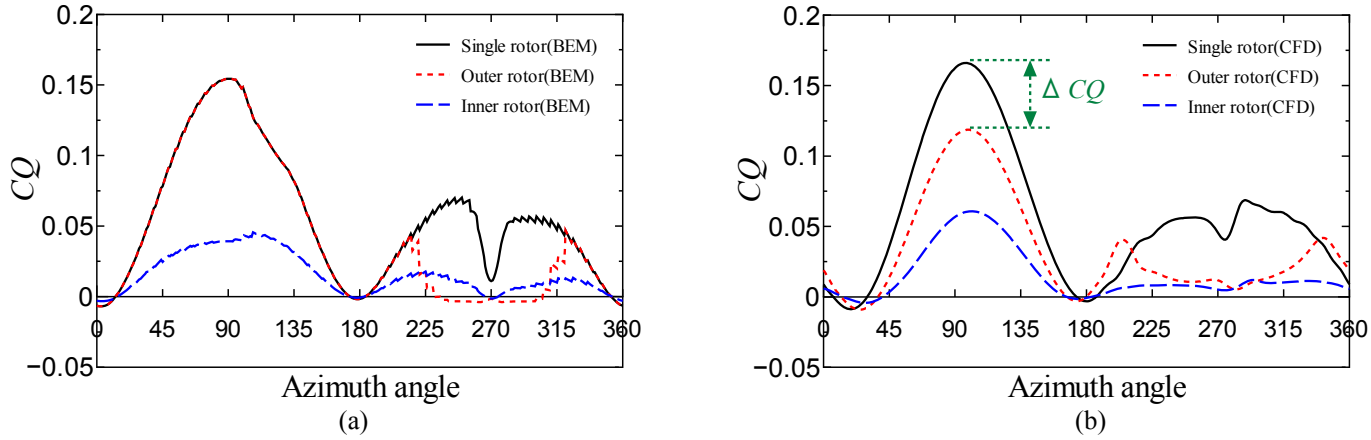

Fig. 11 Blade torque coefficient CQ of double-blade rotor with $\lambda = 3$ (case A, b/R = 0.75) predicted by (a) BEM-QMS and (b) CFD

due to the inner rotor. The CQ of the outer rotor predicted by CFD is smaller than the CQ of the single rotor in the upstream half-cycle. However, BEM-QMS and CFD predict similar torque variations in the downwind half-cycle.

3.2 Modification of the QMS Model

The difference between the maximum blade torque coefficient (in the upwind half-cycle) predicted by CFD for the outer rotor and that for the single rotor, ΔCQ, depended on the value b/R. The value ΔCQ differed between case A (c_1/R = 0.1) and case B (c_1/R = 0.2). The maximum blade torque approximately depends on the square of upstream wind speed V_0. Because the inflow into the double-blade rotor is decreased by the existence of an inner rotor, we assume a virtual upstream-velocity drop ΔV_0 equivalent to the decrease in the maximum blade torque $Q_{out}^{\max}$ of the outer rotor. If a common constant C is introduced, the maximum blade torque of the single rotor $Q_s^{\max}$ and that of the outer rotor $Q_{out}^{\max}$ are assumed to be given by the following equations:

$$Q_s^{\max} \approx CV_0^2 \tag{15}$$

$$Q_{out}^{\max} \approx C(V_0 - \Delta V_0)^2 \tag{16}$$

Using eqs. (14)–(16), ΔCQ can be approximately related to $\Delta V_0 / V_0$ as follows:

$$\Delta CQ = \frac{Q_s^{\max} - Q_{out}^{\max}}{0.5\rho V_0^2 DR} \approx \frac{C\left(2V_0\Delta V_0 - \Delta V_0^2\right)}{0.5\rho V_0^2 DR} = C'\left\{2\frac{\Delta V_0}{V_0} - \left(\frac{\Delta V_0}{V_0}\right)^2\right\} \approx C''\frac{\Delta V_0}{V_0} \tag{17}$$

In the eq. (17), C' and C'' are constants. Because ΔCQ is attributed to the existence of the inner rotor, it should be related to not only the inner-outer radius ratio b/R but the solidity of the inner rotor which is defined by $\sigma_{in} = Zc_2 / b$ where Z is the number of blades.

Figure 12 shows the dependence of $\Delta CQ/\sqrt{\sigma_{in}}$ on b/R. The relationship between $\Delta CQ/\sqrt{\sigma_{in}}$ and b/R seems to be almost linear, except the cases of λ=2 of case A and λ=4 of case B. The broken line depicted in Fig.12 is given by the following equation:

$$\frac{\Delta CQ}{\sqrt{\sigma_{in}}} = 0.103\frac{b}{R} - 0.0151 \tag{18}$$

Using eqs. (17) and (18), we assume the following relationships:

$$\frac{\Delta V_0}{V_0} \propto \Delta CQ \approx \sqrt{\sigma_{in}}\left(0.103\frac{b}{R} - 0.0151\right) \tag{19}$$

Note that eq. (19) is valid when the inner-outer radius ratio b/R is larger than 0.147. To account for these assumptions, eq. (5) is multiplied by a factor f_C as follows:

$$V_1 = V_0 f_C \left(1 - a_1\right) \tag{20}$$

$$f_C = 1 - \frac{\Delta V_0}{V_0} = 1 - k_C \sqrt{\sigma_{in}} \left(0.103 \frac{b}{R} - 0.0151 \right) \tag{21}$$

where k_C is a constant. Although the constant k_C should be determined from experimental data, the value was set at $k_C = 2.0$ on the basis of CFD predictions. We note that the expression of eq. (21) was determined for the case $Z = 3$ and the possibility that the numerical values (0.103 and -0.0151) in eq. (21) depends on the number of blades Z has not been ruled out here.

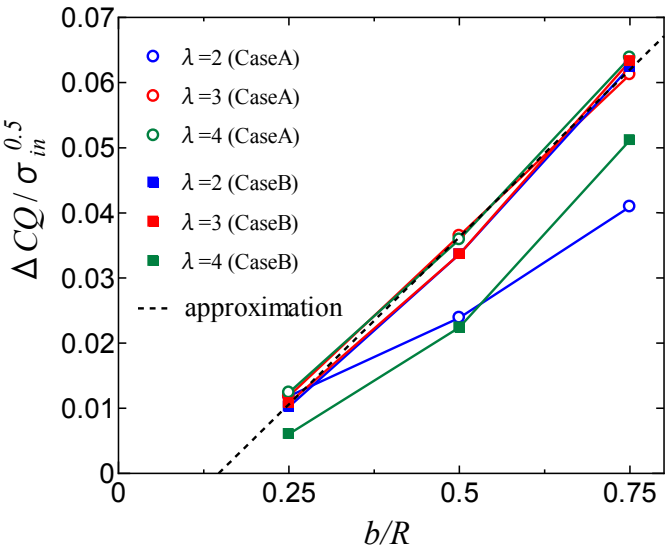

Fig. 12 Dependence of $\Delta CQ/\sqrt{\sigma_{in}}$ on b/R

3.3 Comparison between Modified BEM-QMS and CFD

The power coefficients calculated by the modified BEM-QMS for cases A and B are compared with the CFD predictions in Fig. 13. Comparing predictions by modified BEM-QMS with the values shown in Fig. 7 shows that the maximum power coefficient at each value of b/R is close to the corresponding value of CFD. The position of the power peak predicted by the modified BEM-QMS shifts toward a low tip speed ratio with increasing b/R. This tendency makes the predictions by modified BEM-QMS closer to the CFD predictions than the original BEM-QMS predictions were.

Figures 14 show the torque coefficients of the outer rotor; it is obvious that the torque curves in Fig. 14 are improved over the curves in Fig. 8. Improvements for high tip speed ratios are especially remarkable.

The torque coefficients predicted by the modified BEM-QMS for the inner rotor are compared with CFD predictions in Fig. 15. The maximum torque coefficient for each b/R is smaller than the original prediction (Fig. 9); this tendency means that the original predictions were closer to CFD predictions on this measure. However, the tip speed ratio predicted for the torque peaks by the modified BEM-QMS is lower than that predicted by BEMS-QMS; as a result, for inner rotor torque characteristics, CFD predictions were better matched by modified BEM-QMS predictions than by BEM-QMS predictions.

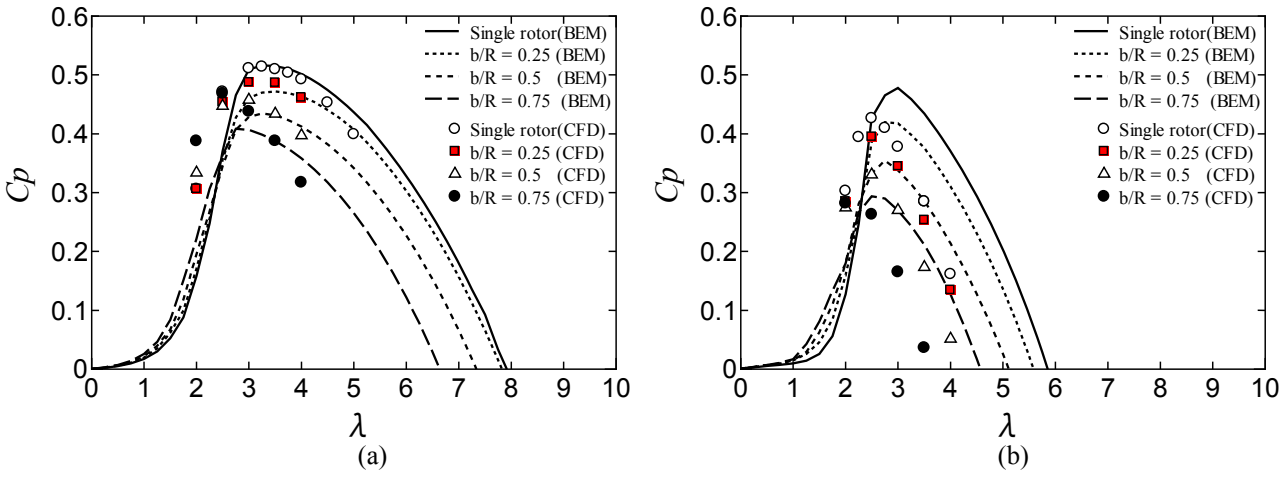

Fig. 13 Total power coefficients from modified BEM-QMS in (a) case A and (b) case B

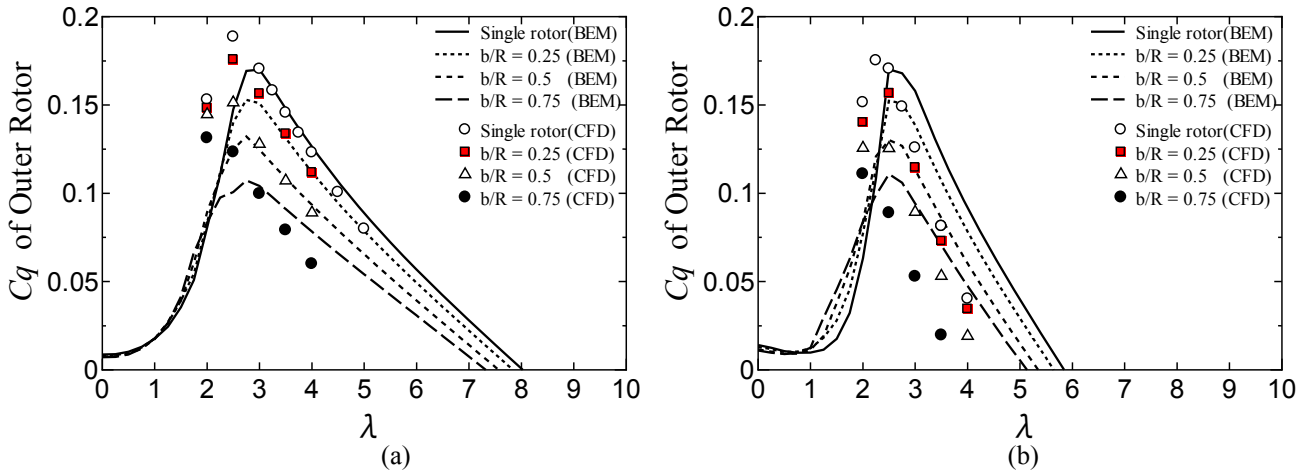

Fig. 14 Torque coefficients of outer rotors from modified BEM-QMS in (a) case A and (b) case B

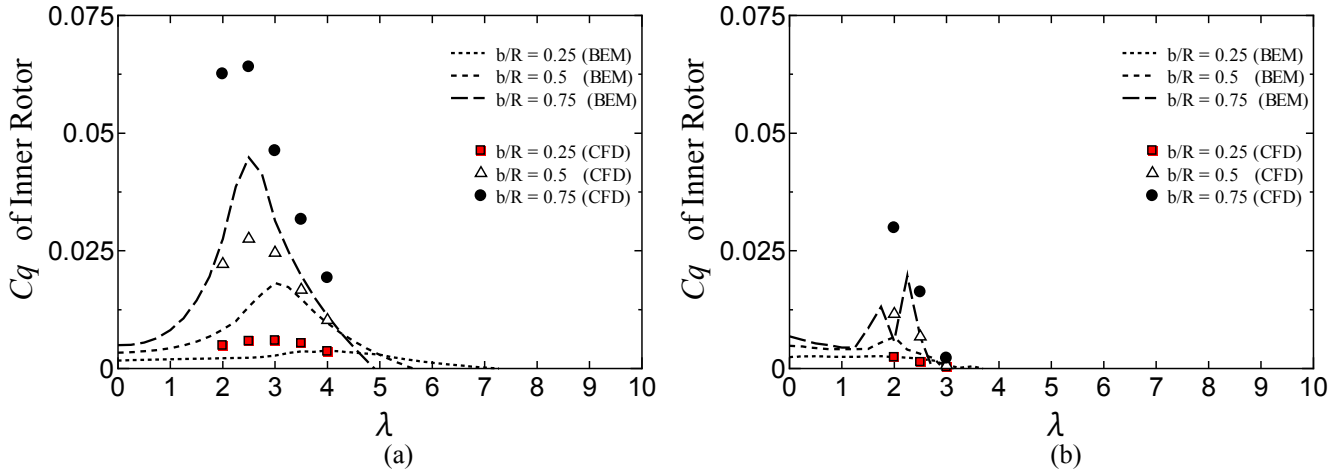

Fig. 15 Torque coefficients of inner rotors from modified BEM-QMS in (a) case A and (b) case B

Figures 16 (a)–(c) show comparisons of blade torque coefficients *CQ* between the modified BEM-QMS and CFD predictions for case A; Figs. 16 (d)–(f) show the same for case B. All the torque variations compared in Fig. 16 were obtained with tip speed ratio 3, and variations in both the outer and the inner rotors are depicted for all inner-outer radius ratios. In both case A and case B, the influence of the inner rotor on the outer rotor torque is apparent in the downwind half-cycle (180° to 360°) and the range of the influence (i.e. the area in which torque decreases) expands with increasing *b*/*R*. The predictions for the outer rotor torque by modified BEM-QMS and CFD agree well in the downwind half-cycle.

In the upwind half-cycle, modified BEM-QMS and CFD agree well on the outer-rotor torque coefficients for azimuth between 120° and 180°, but for azimuth between 0° and 120° the difference in predictions is large. This was previously seen in the single rotor case (Fig. 10). The difference is particularly conspicuous in case B, and the discrepancy between predictions of the modified BEM-QMS and CFD increases with increasing *b*/*R*. As mentioned above, although the cause of the difference in this azimuth range is not clear, the effects of secondary flow and dynamic stall model are candidates. We plan to continue investigating the causes of such differences and further improving the BEM-QMS model in the future.

The differences are large between modified BEM-QMS and CFD for variations in inner-rotor torque, shown in Fig. 16. However, the tendency of inner rotor *CQ* to increase with increasing *b*/*R* is apparent. The smaller the tip speed ratio becomes, the stronger the effect. As shown in Figs. 15 and 13, in the low tip speed ratio range, the inner rotor torque and overall rotor power increase with increasing the inner-outer radius ratio, and this improves the self-starting performance of double-blade rotors.

4. Conclusion

To predict the performance of DB-VAWTs, a new flow model was proposed for the BEM theory; this QMS model uses a nested model based on the conventional DMS model. From the results of comparisons between CFD analysis and BEM-QMS analysis, it was determined that the effects of the inner rotor on the decrease in upstream velocity must be included. To accomplish this, the original BEM-QMS model was modified by introducing a correction factor f_c to the upstream velocity. Modified BEM-QMS showed improved agreement with CFD. Both versions of BEM-QMS predicted an improvement in self-starting for a double-blade rotor at low tip speed ratios, especially when increasing the ratio of the inner rotor radius to the outer rotor radius.

However, the blade torque coefficients predicted by the modified BEM-QMS for azimuth between 0° and 120° (upwind side) differed from those predicted by CFD; this occurred for the single rotor case as well. The cause of this difference is not yet clear. In this study, the BEM-QMS model was compared with only CFD. The effect of changing the number of blades or varying the chord length was not investigated. Further verification of the model by comparison with experimental data and further improvements to the model are still necessary.

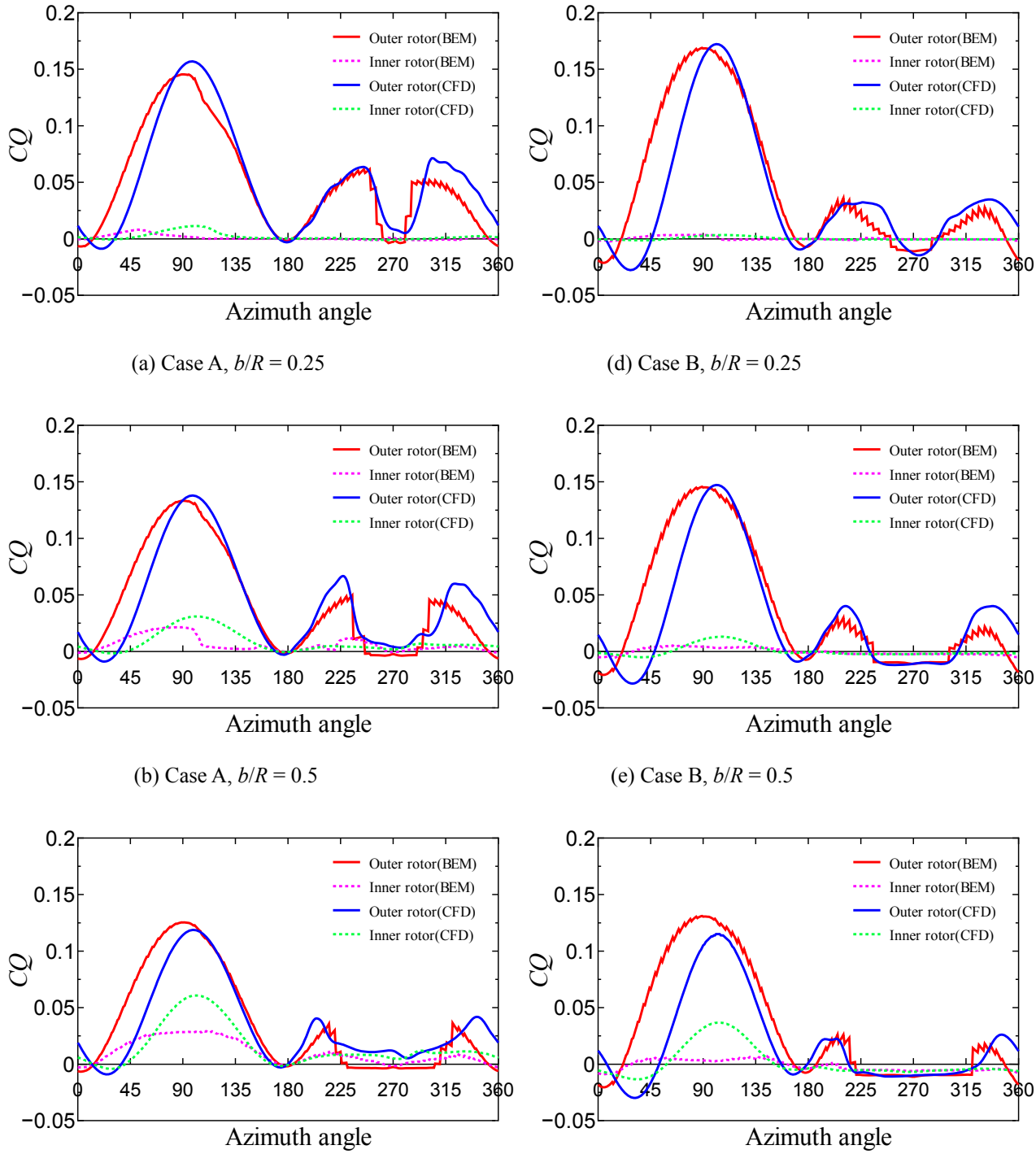

(a) Case A, $b/R = 0.25$

(d) Case B, $b/R = 0.25$

(b) Case A, $b/R = 0.5$

(e) Case B, $b/R = 0.5$

(c) Case A, $b/R = 0.75$

(f) Case B, $b/R = 0.75$

Fig. 16 Comparison between modified BEM-QMS and CFD predictions for CQ when $\lambda = 3$

Acknowledgments

This work was partially supported by JSPS KAKENHI Grants-in-Aid for Scientific Research Nos. 23561031 and 24656528, by the Tottori Prefecture Project for Promoting Environmental Research, and by the Tottori University president's budget.

Nomenclature

A_M	Constant of dynamic stall model	V_0	Upstream velocity [m/s]
a_i	Induction factors (i=1, 2, 3)	V_i	Induced velocity (i=1, 2, 3, 4) [m/s]
b	Radius of inner rotor [m]	V_{eij}	Equilibrium-induced velocity (ij=12, 23, 34) [m/s]
C, C', C''	Constants	V_W	Wake velocity [m/s]
C_p	Rotor power coefficient	W	Relative velocity [m/s]
CQ	Torque coefficient of a blade	Z	Number of blades
c	Chord length [m]	α	Angle of attack [deg.]
c_1	Chord length of outer rotor blade [m]	β_1	Pitch angle of outer rotor blade [deg.]
c_2	Chord length of inner rotor blade [m]	β_2	Pitch angle of inner rotor blade [deg.]
D	Diameter of outer rotor (= 2R) [m]	λ	Tip speed ratio (=$R\omega/V_0$)
D_a	Diameter of rotational axis [m]	ν	Kinematic viscosity [m^2/s]
f_C	Correction factor	ρ	Air density [kg/m^3]
k_C	Constant of upwind-flow speed reduction	σ_{in}	Solidity of inner rotor (=Zc_2/b)
Q	Torque acting on a unit-height blade [Nm]	ψ	Azimuth [deg.]
$Q_{out}^{\max}$	Maximum blade torque of outer rotor [Nm]	ψ_b	Azimuth of inner rotor blade [deg.]
$Q_s^{\max}$	Maximum blade torque of single rotor [Nm]	ψ_R	Azimuth of outer rotor blade [deg.]
R	Radius of outer rotor [m]	ω	Turbine rotational speed [rad/s]
Re	Local Reynolds number (= Wc/ν)		

References

[1] Islam, M., Ting, D. S-K., and Fartaj, A., 2007, "Desirable Airfoil Features for Smaller-Capacity Straight-Bladed VAWT," Wind Engineering, Vol. 31, No. 3, pp. 165-196.

[2] Tanino, T., Nakao, S., Miyaguni, T., and Takahashi, K., 2011, "Influence of Reynolds Number and Scale on Performance Evaluation of Lift-type Vertical Axis Wind Turbine by Scale-model Wind Tunnel Tests," International Journal of Fluid Machinery and Systems, Vol. 4, No. 2, pp. 229-234.

[3] Hara, Y., 2012, "Proposals for Butterfly Wind Turbine and Quadruple-Multiple Streamtube Model," Mechanical Engineering Congress, 2012 Japan (MECJ-12), DVD-No.12-1, S051042 (in Japanese).

[4] Akimoto, H., Tanaka, K., and Uzawa, K., 2011, "Floating Axis Wind Turbines for Offshore Power Generation (A Conceptual Study)," Environmental Research Letters, Vol. 6, No. 4, 044017.

[5] Paulsen, U. S., Vita, L., Madsen, H. A., Hattel, J., Ritchie, E., Leban, K. M., Berthelsen, P. A., Carstensen, S., 2012, "1st Deep Wind 5 MW Baseline Design," Energy Procedia, Vol. 24, pp. 27-35.

[6] Sutherland H. J., Berg D. E., Ashwill T. D., 2012, "A retrospective 1 of VAWT technology," SAND 2012-0304.

[7] Akimoto, H., Nakamura, T., Mizumukai, K., and Hara, Y., 2012, "New Concept of Floating Axis Wind Turbine Assisted by a Savonius Turbine in Water," 1st Asian Wave and Tidal Conference (AWTEC 2012), Jeju Island, Korea, B2-4.

[8] http://vertaxwind.com/ (last retrieved 2013/4)

[9] http://www.verticalwind.se/EN/index.html (last retrieved 2013/4)

[10] http://www.floatingwindfarms.com/ (last retrieved 2013/4)

[11] Paraschivoiu, I., 2002, Wind Turbine Design with Emphasis on Darrieus Concept, Polytechnic International Press.

[12] Migliore, P. G., Wolfe, W. P., and Fanucci, J. B., 1980, "Flow Curvature Effects on Darrieus Turbine Blade Aerodynamics, " J. ENERGY, Vol. 4, No. 2, No.79-0112R, pp. 49-55.

[13] Furukawa, A., Takamatsu, Y., Takenouchi, K., 1990, "Theoretical Considerations in an Approximate Method for Estimating the Blade Performance of a Darrieus-Type Cross-Flow Water Turbine," Mem. Fac. Eng., Kyushu Univ., Vol. 50, No. 1, pp. 1-14.

[14] Sheldahl, R. E. and Klimas, P. C., 1981, "Aerodynamic Characteristics of Seven Symmetrical Airfoil Sections Through 180-Degree Angle of Attack for Use in Aerodynamic Analysis of Vertical Axis Wind Turbines," SAND 80-2114.

[15] Kumar, V., Paraschivoiu, M., Paraschivoiu, I., 2010, "Low Reynolds Number Vertical Axis Wind Turbine for Mars," Wind Engineering, Vol. 34, No. 4, pp. 461-476.

[16] Berg D. E., 1983, "An Improved Double-Multiple Streamtube Model for the Darrieus-Type Vertical Axis Wind Turbine," Sixth Biennial Wind Energy Conference and Workshop, Minneapolis, NM, pp. 231-238.

[17] Wilson, R.E., Walker, S.N., 1981, "Fixed-Wake Analysis of the Darrieus Rotor," SAND 81-7026.